Cavity-enhanced laser spectroscopic studies of vibrational overtones of acetylene

Markus Metsälä

University of Helsinki

Department of Chemistry

Laboratory of Physical Chemistry

P.O. Box 55 (A.I. Virtasen aukio 1)

FIN-00014 University of Helsinki, Finland

Academic dissertation

To be presented, with the permission of the Faculty of Science of the University of Helsinki for public criticism in the Main lecture hall A110 of the Department of Chemistry (A.I. Virtasen aukio 1, Helsinki) June 7th, 2006, at 12 o'clock.

Helsinki 2006

Supervised by:

Professor Lauri Halonen

Department of Chemistry

University of Helsinki

Reviewed by:

Professor Jouko Korppi-Tommola

Department of Chemistry

University of Jyväskylä

and

Docent Åsa Lindberg

Department of Physical Sciences

University of Helsinki

Discussed with:

Professor Gerard Meijer

Department of Molecular Physics

Fritz-Haber-Institut der Max-Planck-Gesellschaft

ISBN 952-92-0381-0 (Paperback)

ISBN 952-10-3168-9 (PDF)

http://ethesis.helsinki.fi

Helsinki 2006

Yliopistopaino

Abstract

This thesis contains five experimental spectroscopic studies that probe the vibration–rotation energy level structure of acetylene and some of its isotopologues. The emphasis is on the development of laser spectroscopic methods for high-resolution molecular spectroscopy.

Three of the experiments use cavity ringdown spectroscopy. One is a standard setup that employs a non-frequency stabilised continuous wave laser as a source. In the other two experiments, the same laser is actively frequency stabilised to the ringdown cavity. This development allows for increased repetition rate of the experimental signal and thus the spectroscopic sensitivity of the method is improved. These setups are applied to the recording of several vibration–rotation overtone bands of both $H^{12}C^{12}CH$ and $H^{13}C^{13}CH$.

An intra-cavity laser absorption spectroscopy setup that uses a commercial continuous wave ring laser and a Fourier transform interferometer is presented. The configuration of the laser is found to be sub-optimal for high-sensitivity work but the spectroscopic results are good and show the viability of this type of approach. Several ro-vibrational bands of carbon-13 substituted acetylenes are recorded and analysed.

Compared with earlier work, the signal-to-noise ratio of a laser-induced dispersed infrared fluorescence experiment is enhanced by more than one order of magnitude by exploiting the geometric characteristics of the setup. The higher sensitivity of the spectrometer leads to the observation of two new symmetric vibrational states of $H^{12}C^{12}CH$. The precision of the spectroscopic parameters of some previously published symmetric states is also improved. An interesting collisional energy transfer process is observed for the excited vibrational states and this phenomenon is explained by a simple step-down model.

Preface

Nothing exists until or unless it is observed. An artist is making something exist by observing it. And his hope for other people is that they will also make it exist by observing it.

William S. Burroughs, 1914-1997

I wish to extend my gratitude to Prof. Lauri Halonen, the supervisor of my thesis. He gave me the initial opportunity to work in his lab years ago and has continued to encourage me during the whole duration of my studies.

I want to also acknowledge my debt to the colleagues in the lab: Dr. Olavi Vaittinen, Dr. Joseph Guss, Dr. Raul Martinez, Dr. Shengfu Yang, Dr. Dmitri Permogorov, Dr. Maria Nela and Mr. Tommi Lantta. Without your help and good humour I would have been doomed to fail. I am also grateful to everyone else at the Laboratory of Physical Chemistry, it has been a nice place to work.

Specifically I want to thank Dr. Olavi Vaittinen and Dr. Janne Pesonen for many seemingly idle coffee breaks and lunches. Our discussions and often heated debates on all things scientific and human kept my desire to understand nature and reality alive even when work in the lab consisted more of aligning optics and soldering resistors than deep scientific contemplation.

Financial support from The Graduate School Laskemo (Ministry of Education) is also gratefully acknowledged.

I do not want to forget my friends, either. I have spent many a moment during the last 20 years with Mr. Skander Chaichee and Mr. Vesa Niininen. Playing football, watching it on TV and generally just enjoying life. Thanks guys.

Finally, I want to dedicate this thesis to Katja, the love of my life and the wisest and most caring person I have ever met. In the end, it was you who opened my eyes to the complex relationship between reality and science.

List of publications

This thesis contains the following publications, which are referred to by the Roman numerals I-V:

I. M. Metsälä, S. Yang, O. Vaittinen, D. Permogorov and L. Halonen, High-resolution cavity ring-down study of acetylene between 12 260 and 12 380 cm^{-1}. Chemical Physics Letters **346**, 373 (2001).

II. M. Metsälä, S. Yang, O. Vaittinen and L. Halonen, Laser-induced dispersed vibration–rotation fluorescence of acetylene: spectra of *ortho* and *para* forms and partial trapping of vibrational energy. Journal of Chemical Physics **117**, 8686 (2002).

III. S. Yang, M. Metsälä, T. Lantta, P. Suero, R. Z. Martinez, O. Vaittinen and L. Halonen, High-resolution Fourier-transform intra-cavity laser absorption study of $H^{12}C^{13}CH$ and $H^{13}C^{13}CH$ at around 12 600 cm^{-1}: A case of strong anharmonic resonances. Chemical Physics Letters **396**, 213 (2004).

IV. R. Z. Martinez, M. Metsälä, O. Vaittinen, T. Lantta and L. Halonen, Laser-locked high-repetition-rate cavity ringdown spectrometer. Journal of Optical Society of America B **23**, 727 (2006).

V. M. Metsälä, J. Guss, O. Vaittinen and L. Halonen, High-repetition-rate cavity ringdown spectroscopy of vibrational overtones of $H^{13}C^{13}CH$ at around 12 600 cm^{-1}. Chemical Physics Letters, in press (2006).

Contents

1 Introduction

Molecular spectroscopy is a discipline of studying the properties of molecules using electromagnetic radiation as a probe. Different parts of the electromagnetic spectrum can be used, with each wavelength range, from centimeter to picometer, corresponding to a different type of molecular phenomenon. These phenomena include transitions between different magnetic components of nuclear spin-states as studied with radio frequency sources (nuclear magnetic resonance) and electronic transitions between different molecular orbitals when visible and ultraviolet sources are used. In this work, I have studied the vibrations and rotations of gas phase molecules that result from stimulation by near-infrared radiation.

Usual spectroscopic studies consist of two different parts. One is the experimental work done to extract empirical information from the molecular sample. This part gives the raw data which, per se, are not more useful than a set of random numbers. For the data to truly reveal the microscopic properties of the molecule, one needs a theoretical model with which to process the information. The match between the data and the model bridges the gap between nature and our abstract conception of it. Without the empirical data, we have no way of testing the model and without the model we have no way of rationalising the data.

The emphasis in this work has been on experimental measurements, but every measurement is accompanied by a set of calculations to analyse the data according to a suitable quantum mechanical model. The primary motivation was to test and improve different experimental techniques used to observe molecular vibration–rotation transitions (i.e. transitions between energy levels associated with vibrational and rotational degrees of freedom of the molecule). These experimental techniques all share common ground in that they exploit the properties of optical cavities to increase the signal-to-noise ratio. A laser is used as a radiation source and either the experiment is conducted inside the laser cavity or the laser beam is coupled into an external optical cavity. The perceived mechanism by which the cavity enhances the experimental signal depends on the application. One can either consider the high optical power gained inside the cavity or the long effective absorption path length imposed by it. These two mechanisms are actually related because the path length and field intensity have an equivalent effect

on the total strength of the excitation of molecular transitions. For the emission experiments conducted in this study, it is easier to look at the enhancement in terms of power while for the absorption experiments it is intuitively the increased path length which brings about the gain in the signal-to-noise ratio. The basic aspects and details of operation of these experimental setups are reviewed in this thesis.

High-sensitivity absorption techniques also have important applications outside research laboratories. The various distinctive absorption features exhibited by all molecules and atoms act as convenient fingerprints in detection of these species. Cavity ringdown spectroscopy (CRDS), which is the technique used and developed in three of the publications in this thesis, is a promising technique for, among others, airborne measurements of atmospheric species, trace detection of explosives [1], human breath analysis [2, 3] and detection of agriculturally important molecules [4]. And even though most CRDS experiments probe absorption of gas phase species, some studies have extended the technique to condensed phases. Successful applications include detection of micro-organisms [5] and incorporating a CRDS spectrometer as a detector in a liquid chromatography experiment [6].

From a molecular point of view, I have been interested in studying the overtone vibration–rotation transitions in acetylene (HCCH) and some of its carbon-13 substituted isotopologues. Acetylene is a widely studied molecule in high-resolution spectroscopy [7] and it is often used as a convenient test system for new experimental methods. The energy level structures of the rarer isotopologues are less well known but global modelling of the vibrational states has also been carried out on these species [8]. The overtone transitions result in appreciably weaker signals than those encountered in spectroscopic measurements of the fundamental vibrations and thus the sensitivity of the experimental technique must be emphasised. On the other hand, the high symmetry in the equilibrium bond structure of acetylene limits the number of accessible vibration–rotation levels in one-photon absorption measurements. Both of these complications are addressed in the experimental techniques used in this work. The spectroscopic results obtained are also treated in this overview part of the thesis, but because the focus of my studies has been on the experimental side, these will be given less weight. I will, however, present a concise description of the quantum mechanical model

used in the analysis of the spectroscopic data, because I feel that it is necessary for a proper understanding of the scientific context of this work.

This thesis consists of five refereed publications, a brief summary of each is given below.

Publication I describes an experiment in which a highly sensitive absorption technique, cavity ringdown spectroscopy, is applied to the overtone spectroscopy of acetylene. The construction of the experimental setup is discussed and different data processing measures are compared. A new set of vibrational states is also observed and this is rotationally analysed.

Publication II addresses the problems associated with the symmetry of acetylene. An emission technique is used to circumvent the normal one-photon selection rules and symmetric vibrational states are thereby accessed. The sensitivity of the experimental setup is enhanced with respect to previous studies. Dynamic effects due to molecular collisions are also observed and a set of hitherto unobserved vibrational states is analysed.

Publication III describes another high-sensitivity absorption technique: Fourier transform intra-cavity laser absorption spectroscopy (FT-ICLAS). A simple setup based on commercial instruments is built with good results. Several new vibration–rotation bands are recorded and analysed for the carbon-13 isotopologues of acetylene: $H^{12}C^{13}CH$ and $H^{13}C^{13}CH$. A set of anharmonic resonances within the observed vibrational states is also rotationally analysed.

Publication IV describes a cavity ringdown experiment where the repetition rate of the ringdown signal is increased by frequency stabilising the laser source to a high-finesse ringdown cavity. A high-resolution digital acquisition system is used to minimise quantisation noise and high-speed processing of the data is performed in order to take full advantage of the sensitivity of the setup.

Publication V concerns the application of the spectrometer developed in the previous publication to vibrational overtones of $H^{13}C^{13}CH$. Several previously unknown overtone states are observed and these are all rotationally analysed. Small experimental improvements to the setup are also discussed. Overall the practical applicability of the spectrometer is demonstrated.

2 Molecular theory

The molecular phenomena relevant to this work are the rotation and vibration of molecules and the transitions between energy levels associated with these degrees of freedom. In the following subsections I will briefly outline the quantum mechanical theory behind these physical processes and I will emphasise the special case of linear molecules, such as acetylene.

2.1 Rotation

The basis for calculating molecular energy levels associated with rotational (and vibrational) motion is the Schrödinger equation. It can be expressed as

$$H\Psi = T\Psi + V\Psi = -\frac{\hbar^2}{2m}\nabla^2\Psi + V\Psi = E\Psi, \tag{1}$$

where ∇^2 is the Laplacian, $\hbar$ is the Planck constant divided by 2π, m is the mass of the system and E is the energy associated with the wavefunction (Ψ) operated by the Hamiltonian (H). The Hamiltonian consists of the kinetic energy part (T) and the potential energy part (V).

According to the Born–Oppenheimer approximation, we can separate the motion of electrons and nuclei in the molecule. This means that it is possible to use a static electronic potential when calculating the energies associated with rotation and vibration. We can also separate the motion of the center of mass (translation) of the molecule from the the overall rotation and relative motion of the atoms. And often we make the approximation that there is no coupling between the rotational and vibrational degrees of freedom so that these can be treated separately.

At first, we assume that the rotational motion of the molecule follows the dynamics of a rigid rotor, that is, the bond lengths of the molecule do not change during rotation. Then, for pure rotation, the Hamiltonian operator is [9]

$$H_r = \frac{J_x^2}{2I_{xx}} + \frac{J_y^2}{2I_{yy}} + \frac{J_z^2}{2I_{zz}}, \tag{2}$$

where J_α is the operator for the αth molecule-fixed Cartesian component of the

total angular momentum and $I_{\alpha\alpha}$ is the principal moment of inertia about an axis α. For a rigid rotor, the potential energy part of the Hamiltonian is absent, there is no change in bond lengths and thus no change in the electron distribution. The total angular momentum operator is given by

$$\mathbf{J} = \mathbf{r} \times \mathbf{p} = \mathbf{r} \times \frac{\hbar}{\mathrm{i}}\nabla, \tag{3}$$

where $\mathbf{r}$ is the position vector, $\mathbf{p}$ is the linear momentum vector and i is the imaginary unit.

The moment of inertia is defined as a function of perpendicular distance of the atom i from the axis α as

$$I_{\alpha\alpha} = \sum_i m_i x_{\alpha i}^2, \tag{4}$$

where m_i is the mass of the atom i.

The general solution of the Schrödinger equation with the Hamiltonian operator H_r will include in principle three quantum numbers, one for each moment of inertia. For a linear molecule, like acetylene, the treatment is simplified. The moment of inertia associated with the molecular axis is zero and the two other principal moments of inertia are identical. The energy level structure for a linear molecule can be expressed as function of the total angular momentum quantum number J

$$E(J)/h = BJ(J+1), \tag{5}$$

where the rotational constant, B, can be described as a function of the moment of inertia along the principal axis perpendicular to the molecular axis ($I_\perp$)

$$B = \frac{\hbar}{4\pi I_\perp}. \tag{6}$$

The model described above is based on the rigid rotor approximation and assumes a fixed symmetry (linear) for the molecule. If the bending vibrations of the molecule are excited, we must include a vibrational angular momentum quantum number in the model to account for the moment of inertia along the molecular axis. Also, if the bonds of the molecule stretch during the rotation, the rigid rotor approximation is no longer valid and an additional term has to

be included in the Hamiltonian to account for this centrifugal distortion effect. The physical origin of this term is the centrifugal force that tends to stretch the molecule and the spring force that opposes this displacement [9]. In equilibrium, these forces are in balance and the energy level structure is given by

$$E(J)/h = BJ(J+1) - DJ^2(J+1)^2, \tag{7}$$

where D is the centrifugal distortion coefficient. As hinted above, D is a function of the harmonic force constant of the bond and for a diatomic molecule is written as

$$D = \frac{4B^3}{\omega^2}, \tag{8}$$

where ω is the vibrational frequency of the rotating system. The stronger the bond the higher the frequency is and the smaller the effect of the centrifugal distortion. On the other hand, a smaller internuclear distance corresponds to a smaller moment of inertia and a larger B constant thus leading to a larger value of D.

The description above has taken into account only the rotational part of the molecular movement. The energy needed to excite these pure rotational transitions is in the microwave region of electromagnetic spectrum. In this thesis, however, the experiments have been conducted in the near-infrared region and no pure rotational transitions have been measured. In the infrared region, the rotational transitions appear as a fine structure within the vibrational energy manifold (see next Section) and the situation differs from the case of pure rotation. First, the rotational parameters are effective to the vibrational state they are associated with. Second, interactions between the rotational and vibrational motions may arise and complicate the model needed to explain the experimental results in a satisfactory manner.

The energy levels are described by the equations given above, but not every transition between any two levels is possible. If the transition moment matrix element of the electric dipole moment operator (as seen in Section 2.3) linking two states is zero, then the transition between these states is not observed. For a linear molecule, the selection rules of rotational fine structure associated with

vibrational transitions are

$$\Delta J = \pm 1 \text{ and } \Delta J = 0, \tag{9}$$

where $\Delta J = J' - J''$, the single and double prime refer to upper and lower state, respectively. The second rule applies only to transitions in which at least one of the states possesses non-zero vibrational angular momentum (see Section 2.2).

The rotational energy level structures of the vibration–rotation overtone bands recorded and analysed in this study have been, for the most part, modelled with equations similar to Eq. 7. In some cases, a high order fitting parameter H has been used in the energy level equation for a better match with the experimental data.

2.2 Vibration

The simplest approach to model molecular vibrations is to assume a harmonic potential for the relative displacements of the nuclei. For a diatomic system, this results in the following Hamiltonian operator

$$H = -\frac{\hbar^2}{2\mu}\frac{\partial^2}{\partial x^2} + \frac{1}{2}kx^2, \tag{10}$$

where x is the relative displacement of the nuclei, k is the force constant of the bond oscillator and μ is the reduced mass of the two nuclei with masses m_1 and m_2 [$\mu = m_1 m_2/(m_1 + m_2)$].

The harmonic approximation results in a uniformly spaced energy level structure given by

$$E(v) = (v + \frac{1}{2})\hbar\omega \quad \omega = \left(\frac{k}{\mu}\right)^{1/2}, \tag{11}$$

where $v = 0, 1, 2, \ldots$ is the vibrational quantum number.

Within the harmonic approximation, the selection rules are such that only optical transitions that change the vibrational quantum number by one ($\Delta v = \pm 1$) are allowed. However, the overtone transitions that I have been investigating in this study involve a change in v by several quanta ($\Delta v = 2, 3, 4, \ldots$). Clearly, the harmonic potential cannot be considered accurate in this context.

One way to proceed is to replace the parabolic potential with a more realistic function like, for example, a Morse function

$$V(x) = hcD_e\left(1 - e^{-ax}\right)^2 \quad a = \left(\frac{k}{2hcD_e}\right)^{1/2}, \tag{12}$$

where c is the speed of light, D_e is the depth of the minimum of the potential energy well and a describes the steepness of the potential. This function models the molecular potential better than a harmonic surface, especially far away from the equilibrium structure. The strict selection rule $\Delta v = \pm 1$ does not apply with a Morse potential and transitions between the ground state and highly excited vibrational states are possible. The shape of the dipole moment surface can also lead to a similar relaxation of the selection rules, this effect is explored further in the next Section. The energy level equation is also modified from the one derived within the harmonic approximation. The levels are not uniformly spaced but given by

$$E(v) = (v + \frac{1}{2})\hbar\omega - (v + \frac{1}{2})^2\hbar\omega x_e \quad \omega x_e = \frac{a^2\hbar}{2\mu}, \tag{13}$$

where ωx_e is the anharmonicity parameter.

A diatomic molecule possesses only one mode of vibrational motion but for a polyatomic molecule the picture is more complicated. For a linear molecule consisting of N atoms, there are a total of $3N - 5$ vibrational modes. These are usually described as normal modes using rectilinear coordinates that diagonalise the matrix representing the harmonic vibrational energies. A list of the normal modes of acetylene [10] is given in Table 1 along with the corresponding experimental wavenumbers [11]. Vibrational motion can also be modelled using other types of coordinates, such as the curvilinear bond stretch and bond angle displacements, which are used in the local mode model [12]. As the degree of vibrational excitation increases, the local mode description can provide a better physical picture of the energy level structure, particularly for the stretching overtones involving hydrogen or deuterium nuclei.

The bending vibrations in acetylene are doubly degenerate and contribute to the total angular momentum of the molecule [7]. This means that one must deduct the vibrational angular momentum quantum number k from the total angular momentum quantum number J when calculating the pure rotational

Notation	Description	Wavenumber / cm^{-1}
1000^00^0	symmetric C-H stretch	3374
0100^00^0	C≡C stretch	1974
0010^00^0	anti-symmetric C-H stretch	3287
0001^10^0	*trans*-bend	612
0000^01^1	*cis*-bend	729

Table 1: Normal mode vibrations of acetylene

energy. Also, as mentioned in the previous Section, for vibrational transitions with $\Delta k \neq 0$, the $\Delta J = 0$ rotational transitions are allowed. Thus, in practice, it is easy to distinguish transitions from the ground state to pure stretching states as opposed to bending states with $k \neq 0$. The transitions obeying the selection rule $\Delta J = 0$ form a characteristically dense spectral feature, so-called Q branch, while the $\Delta J = 1$ and $\Delta J = -1$ transitions group as R and P branches, respectively, on either sides of the Q branch. A missing strong Q branch is a sign of a vibrational transition where the change in vibrational angular momentum quantum number is zero ($\Delta k = 0$). A weak Q branch can also be observed for transitions between bending states when $\Delta k = 0$ but $k' = k'' \neq 0$.

A realistic state-of-the-art model for the vibrations of a polyatomic molecule, such as acetylene, is quite involved [7, 13]. The interactions between different states become significant and the resulting energy level pattern is complicated, especially in the overtone region, where several quanta of vibrations are excited. One must then abandon the simple model where all the vibrations are treated separately and include interactions between states as perturbations in the vibrational model. In Publication V, I made a vibrational calculation for the $H^{13}C^{13}CH$ isotopologue based on the diagonal and off-diagonal matrix elements of the Hamiltonian operator given by Di Lonardo *et al.* [8]. This calculation was used to assign vibrational labels to a set of observed states. The assignment was made based not only on the calculated vibrational energy but also on the predicted rotational B constant. The latter is sensitive to the composition of the eigenstate and helps in the assignment procedure.

2.3 Optical transitions

In the previous sections, I outlined the energy level structures generated by the rotational and vibrational degrees of freedom of acetylene. I also mentioned that transitions between these different states may be possible. This section describes the physical process that makes these transitions occur.

The energy level equations for rotation and vibration are based on the solutions to the time-independent Schrödinger equation. A time-dependent perturbation has to be included to induce transitions between states. In our case, it is convenient to make this perturbation an oscillating function with frequency ω. The perturbation then corresponds to a classical electromagnetic field. When the oscillation frequency matches the energy separation of two molecular states ($\Delta E = \hbar\omega$), the resonant transition rate between states a and b can be given by

$$R_{ab} \sim \left| \frac{V_{ba}^0}{\hbar} \right|^2 g(\omega_{ab}), \tag{14}$$

where V_{ba}^0 is a term describing the interaction between the perturbing oscillation and the molecule, and $g(\omega)$ is the distribution of frequencies present in the perturbing field. What remains to be specified is the physical form and meaning of V_{ba}^0, and how the transition rate relates to the absorption and emission processes observed in the laboratory.

It turns out that the first-order contribution in the interaction between the optical field and the molecule is between the electric part of the field and the dipole moment operator of the molecule [14]. If the electric field in three dimensions is written as

$$\mathcal{E}(\mathbf{r}, t) = \mathbf{E_0} \cos(\omega t - \mathbf{k} \cdot \mathbf{r}), \tag{15}$$

then the electric dipole interaction operator is

$$\mathcal{H}(t) = \mathcal{E}(\mathbf{r}, t) \cdot \boldsymbol{\mu} = \mathcal{E}(\mathbf{r}, t) \cdot (\sum_i q_i \mathbf{r_i}), \tag{16}$$

where the sum over i includes all the charges q_i in the molecule, and $\mathbf{k}$ and $\mathbf{E_0}$ are the propagation vector and the electric field vector, respectively.

One can use Eq. 16 to determine the interaction term V_{ba}^0, and the transition

rate for a resonant field becomes [14]

$$R_{ab} = \frac{\pi}{2\hbar^2}|E_0|^2|\langle b|\boldsymbol{\mu}|a\rangle|^2 = \frac{\pi}{2\hbar^2}|E_0|^2\mu_{ab}^2, \tag{17}$$

where the expression in brackets is a matrix element of the dipole moment operator. If the matrix element μ_{ab} is non-zero, then the transition is possible provided that the optical field possesses spectral density at the resonant frequency ω_{ab}. As the first order contribution in the interaction between the optical field and the molecule, the electric dipole moment is responsible for the strongest molecular transitions. If the matrix element for the dipole moment operator is zero, weaker effects due to the possible non-zero electric quadrupole moment or magnetic dipole moment can still contribute to the observed transition intensity.

To relate the matrix elements to the absorption and emission intensities observed in standard spectroscopic experiments, one needs to take into account the different processes by which the transitions can occur. To derive a general steady-state equation for absorption, not only must the transition rate for stimulated absorption be included but also the rates for both stimulated and spontaneous emission, and the rates for any non-radiative processes that may take place. The radiative processes are quantitatively described by the phenomenological Einstein coefficients A and B. The quantity A is the spontaneous emission rate coefficient and B is the rate coefficient for both stimulated absorption and stimulated emission when the upper and lower levels of the transition are non-degenerate. Unsurprisingly, B is related to the matrix element of the dipole moment operator

$$B_{ab} = \frac{\mu_{ab}^2}{6\varepsilon_0\hbar^2}g(\nu - \nu_{ab}), \tag{18}$$

where ε_0 is the permittivity of vacuum, $g(\nu - \nu_{ab})$ is the lineshape function of the transition and B_{ab} refers to the rate coefficient connected with the transition between states a and b.

To arrive at an equation that describes the attenuation experienced by an optical field passing through the sample, the assumption has to be made that the radiation field is weak enough not to appreciably perturb the equilibrium population of the lower and upper states. The spontaneous emission rate from the upper state to the lower is also ignored. The upper state population N_b remains non-significant compared to the lower state population N_a so that the

absorption rate can be expressed as

$$-\frac{dN_a}{dt} = B_{ab}(N_a - N_b)\rho \approx B_{ab}N_a\rho, \tag{19}$$

where ρ is the energy density of the optical field.

We can now write an expression for the field intensity I [W/cm^2] passing through an infinitesimal length of sample dl as [14]

$$-\frac{dI}{I} = \frac{h}{c}\nu_{ab}B_{ab}N_a\,dl = \alpha\,dl, \tag{20}$$

where ν_{ab} is the vibrational frequency, α is the molecular absorption coefficient for this specific transition. Eq. 20 is effectively the same as the familiar Lambert-Beer law for linear absorption in the weak field regime.

The above equations assume that the transition strength is distributed to only one absorption line. However, as discussed in Section 2.1, the vibrational bands contain rotational fine structure and thus the intensity of the vibrational transition is distributed among these rotational lines. Several factors must be accounted for to calculate the vibrational transition moment based on observed intensities of individual rotation–vibration lines. The relative lower state population has to be calculated and the Hönl-London factor [10] must be included. This factor takes into account how the intensity is distributed between the Q, R and P branches and between different J values. Such an intensity analysis is performed in Publication V.

One can exploit the symmetry of the molecule to derive vibrational selection rules from group theory. The matrix element of the transition dipole moment will be non-vanishing only if the total product of the dipole moment operator with the wavefunctions of the upper and lower states contains the totally symmetric representation. In the case of acetylene, this means that only two of the five fundamental vibrations are allowed electric dipole transitions [11]. The rest can be observed in Raman experiments which probe the polarisability of the molecule. These selection rules, however, tell us only whether the transition is allowed or forbidden, the intensity of allowed infrared transitions must be calculated from the matrix elements of the dipole moment operator.

The smaller the magnitude of a specific matrix element is, the harder it is to

observe the corresponding transition experimentally. This is important within the framework of this study, because the transition moments of vibrational overtones become drastically smaller as more and more vibrational quanta are excited. The overtone dipole moment transitions are strictly forbidden within the harmonic oscillator approximation and become possible only when anharmonicity is included in the molecular description. This anharmonicity can be either mechanical or electrical. In a mechanically anharmonic system, the potential energy function of the molecule is not harmonic and has to be modelled using, for instance, the Morse potential described in Section 2.2. Electrical anharmonicity, on the other hand, means that the Taylor expansion of the dipole moment function includes terms beyond the linear part. In either case, the overtone transitions are possible but their transition moments become smaller and smaller as the transition frequency increases.

3 Experiments

All the experiments in this study have been performed with the same main instruments. The near-infrared laser source is the Coherent 899-21 Ti:Sapphire ring laser which is optically pumped either by a Coherent Verdi (Nd:YVO_4) solid-state laser or a Coherent Argon-ion gas laser. A Bruker IFS-120 high-resolution Fourier transform interferometer has also been employed to spectrally analyse the fluorescence spectra in the emission study and the laser output in the intra-cavity laser absorption experiment.

The Ti:Sapphire laser has an output range of 700 nm – 1000 nm through the use of three sets of cavity mirrors and its maximum output power is about 1 W (with 10 W of pumping power), depending on the wavelength region. The linewidth of the laser is about 20 MHz when operated in the single mode configuration with all the frequency selective components installed in the cavity. The linewidth can be further reduced to about 1 MHz by using the active frequency stabilisation loop included with the laser.

The maximum instrumental resolution of the interferometer is 0.0015 cm^{-1} for single-sided interferograms. When operated in emission mode, it is preferable to record double-sided interferograms, in which case the maximum instrumental resolution is 0.02 cm^{-1}. It is impossible to use the customary Mertz phase cor-

rection method with narrow band sources in emission mode, and therefore the whole symmetrically sampled interferogram must be recorded to calculate the magnitude spectrum [15].

3.1 Absorption techniques

In the following sections, I will outline the experimental techniques used in this study to obtain direct one-photon absorption spectra. The main principles and features of the different techniques will be presented and special emphasis will be placed on aspects that are relevant to the experimental setups constructed in this study.

3.1.1 Cavity ringdown spectroscopy

Cavity ringdown spectroscopy (CRDS) is a technique that was conceived less than 20 years ago [16] and has increased in popularity in recent years [17]. The central idea is to trap a pulse of laser light between two or more highly reflective mirrors and observe the time decay of the laser intensity. At each round trip between the mirrors, a fraction of the photons is transmitted. A first-order differential equation for the time dependence of the intensity leaking from the cavity can be presented as follows

$$\frac{dI}{dt} = \frac{-Tc}{L} I, \tag{21}$$

where I is the intensity, T is the transmission of the mirrors and L is the cavity length. In the absence of any other loss mechanisms (e.g. scattering) inside the mirrors, the reflectivity R and transmission T are related by $T = 1 - R$. The basic configuration of a CRDS setup is shown schematically in Figure 1.

Instead of a vacuum, a molecular absorber can be placed inside the cavity. A similar term to that for the mirror transmission must then be included for molecular absorption. The total coefficient for the photon loss in each round trip is then $\alpha L + T$, where α is an absorption coefficient. Eq. 21 can be integrated and the time dependence of the intensity can be written as

$$I(t) = I_0 \exp\left(-t/\tau\right) \quad \tau = \frac{L}{c(T + \alpha L)}. \tag{22}$$

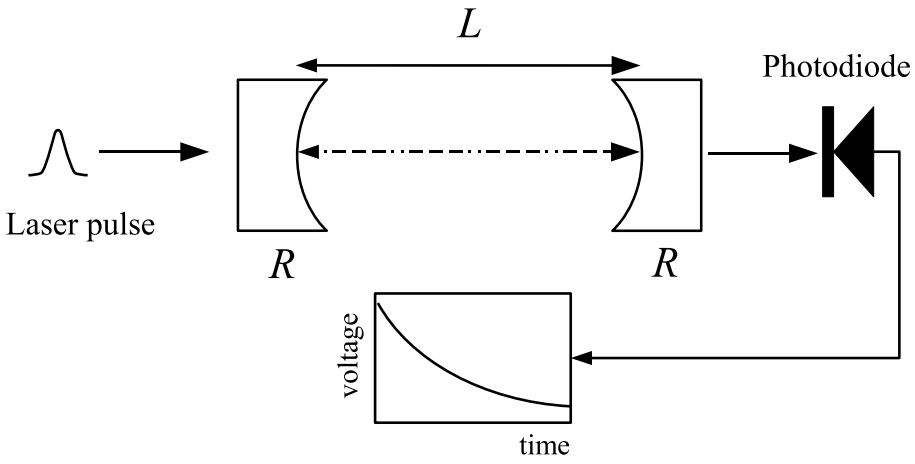

Figure 1: Schematic picture of a CRDS experiment. A laser pulse is directed to an optical cavity of length L consisting of two mirrors with reflectivities R. The exponential decay of light intensity is recorded with a photodiode.

Thus, the decay follows an exponential function with a time constant τ that is inversely proportional to the sum of the mirror transmission and the molecular absorption. Most importantly, the time constant is independent of the amplitude of the exponential and is therefore not influenced by intensity fluctuations in the laser beam. The inherent high sensitivity of the technique is due to the large number of reflections the photons experience before they leak out of the cavity. Because the sample is also contained between the mirrors, the effective absorption path length becomes longer as the reflectivity of the mirrors is increased. In practice, the change in the exponential time constant (relative to an empty cavity) becomes larger as the reflectivity of the mirrors increases. The quality factor of the cavity can be expressed either by the reflectivities of the mirrors or by the so-called finesse of the cavity, $F = \pi\sqrt{R}/(1-R)$.

The frequency response of the cavity is not covered by the simple model presented above. The steady-state model is the standard Fabry-Perót etalon theory that predicts a frequency comb with periodic longitudinal resonances in frequency space [18]. These resonances are uniformly spaced, the difference in frequency being the free spectral range (FSR), $\Delta f = c/(2L)$. It turns out that this steady-state model is also valid in the limit of short laser pulses injected into the cavity [19]. To achieve the best possible sensitivity in a CRDS experiment, care has to be taken that only one mode of the cavity is excited. If the laser linewidth is

larger than the spacing of any two longitudinal or transverse cavity modes, these modes can be excited simultaneously. And if the time constant is different for the frequencies of these modes, the resulting decay will not be mono-exponential. The linewidth of continuous wave (cw) lasers is usually narrower than the longitudinal mode spacing and this problem is not encountered in cw experiments. However, it is still necessary to spatially match the injected laser beam to the lowest transverse mode of the cavity so that no higher order transverse modes are excited.

The first version of CRDS that was implemented in this study (see Publication I) was based on the use of a free-running cw laser to feed the ringdown cavity. This approach poses two problems. The first one is the narrow linewidth of a cw laser, about 20 MHz for our Ti:Sapphire ring laser. The longitudinal mode spacing for normal sized cavities ($\approx$ 50 cm) is in the order of hundreds of MHz. This means that when the laser frequency is scanned, most of the time the laser will not be in resonance with the cavity. This might result in missed spectral features if the FSR is large enough. The second problem is such that a clean exponential decay is not observed if laser light is continuously injected into the cavity for an indefinite amount of time. Instead, the response will be a complex feature that corresponds to the instantaneous laser frequency moving on and off the narrow cavity resonance at random intervals.

Following the work of Romanini *et al.* [20], the problems described above are solved by adding two devices into the setup. The first one is an acousto-optic modulator (AOM) that is used to cut the path of the laser beam once a certain intensity level is reached inside the cavity. This is done by aligning the first order maximum of the AOM to the cavity and then turning the AOM off at an appropriate instant. The second device is a piezo ceramic tube that is attached to one of the cavity mirrors. By applying an AC voltage across the electrodes of the piezo tube, the length of the cavity and the positions of the cavity modes in frequency space are modulated. If the frequencies of the cavity modes are modulated by at least one FSR, the laser frequency matches a cavity resonance periodically and no spectral features will be missed.

Once the exponential intensity decay is observed, one is left with the task of extracting the time constant from the experimental data. There are two basic ways to achieve this. With the computing power available nowadays, a straight-

forward way is to digitise the signal and then fit an exponential function to the resulting digital data. Different fitting algorithms can be used and the quality of the time constant is found to depend slightly on the chosen algorithm. For the simulated data in Publication I, the most consistent fitting results were obtained with a non-linear least squares fit to an exponential function. A second approach is to keep analog data in its original domain and to extract the time constant using only analog manipulations. Lehmann and Romanini did this by effectively integrating the decays using two box-car integrators [21]. Alternatively, a logarithmic amplifier and a subsequent differentiator can be used to first linearise the signal (taking a logarithm of an exponential) and then to obtain the derivative and thus the time constant of the decay [22]. The main advantage of an analog data acquisition system is that there is no digitisation noise imposed by the limited resolution of the analog-to-digital converter. Also, if high repetition rates are achieved for the ringdown events, the digital acquisition system might be unable to process all the data in real time.

High repetition rates are not a concern in normal cw-CRDS experiments such as the one described in Article I. This is due to the relatively poor coupling efficiency of the cw beam into the ringdown cavity. The faster one modulates the cavity, the higher the slope of the modulation signal and the smaller the coupling efficiency is. In normal circumstances, one is limited to modulation frequencies of hundreds of hertz, at most. This relaxes the demands imposed on the data acquisition system but, on the other hand, also limits the achievable sensitivity. An experimental setup with a high repetition rate allows for more averaging of signal data per time unit and consequently provides a better signal-to-noise ratio for a given time limit.

High-repetition-rate CRDS To increase the coupling efficiency, the time the laser beam spends on resonance with the cavity has to be extended. Normally, there is no control over this parameter, it is simply dictated by the statistical frequency noise of the laser. For standard commercial free running lasers, the frequency noise is several orders of magnitude larger than the cavity resonance width of a high finesse ringdown cavity. To decrease the noise level, one can develop an active stabilisation system that locks the laser frequency to a cavity resonance. This means correcting the instantaneous changes in laser frequency

using negative feedback from the external cavity. With such a frequency stabilisation scheme, the cw laser beam can be constantly coupled into the cavity, that is, the linewidth of the laser can be decreased below the linewidth of the cavity. With a fast optical switch, an AOM for example, the radiation field inside the cavity can be turned on and off and the exponential ringdown decays can be observed with a high repetition rate [23].

A frequency stabilisation system requires an error signal to provide feedback to the laser system. The error signal can be derived in many ways. In a standard procedure, the output of the external cavity is monitored and the transmission point about half way up the cavity fringe is used as a reference [24]. When the laser frequency drifts to either side of this point, the transmission is either increased or decreased with respect to the reference. This amounts to a signal with a zero point and a different sign on either side of the zero. The signal can then be supplied to the frequency correcting servo elements for stabilisation. The problem with such a setup is that the bandwidth is limited by the storage time of the cavity, in effect the photons pass through the cavity only after a delay. The higher the reflectivity of the cavity mirrors, the longer the delay is. On the other hand, for maximum sensitivity of the stabilisation loop, a narrow transmission feature is desirable and thus a high-finesse cavity is necessary. To obtain an error signal with good contrast, one must sacrifice bandwidth and vice versa.

Another possibility is to use the Pound-Drever-Hall stabilisation scheme [25], where the error signal is derived from a reflection off the input mirror of the cavity. The laser beam is phase modulated with an electro-optic modulator (EOM) before the cavity, thus producing frequency sidebands on each side of the carrier. The error signal is generated essentially from the instantaneous phase imbalance between the two sidebands and the carrier in the reflected beam. The sign of the error signal is different on the opposite sides of the cavity fringe and is zero at the maximum transmission point. This makes the signal suitable for stabilisation purposes as the lock point will be at the maximum transmission and, if the laser frequency veers to either side of the maximum, the error signal will be of appropriate sign to move it back. Because the feedback signal is derived from back-reflected light from the cavity, there is no limit to the available bandwidth.

In Article IV of this work, the Pound-Drever-Hall scheme is applied to a Ti:Sapphire ring laser. The laser is stabilised to a cavity with finesse of about

18 000. The feedback system utilises three different servo actuators to control the laser frequency with a total bandwidth of about 200 kHz. An intra-cavity quartz plate, attached to a galvanometric motor, handles the slowest perturbations (DC to 50 Hz). The next two decades (50 Hz to 10 kHz) are sent to a piezo ceramic element that is attached to one of the mirrors in the laser cavity. The fastest error signals are fed to an external AOM that corrects frequency excursions between 10 kHz and 200 kHz. The gain function of the feedback electronics is a first order integrator for both the galvo and AOM channels. To boost the closed loop gain at lower frequencies, a second order integrator function is applied to the signal sent to the piezo ceramic element. Fig. 2 is a schematic picture of the stabilisation setup.

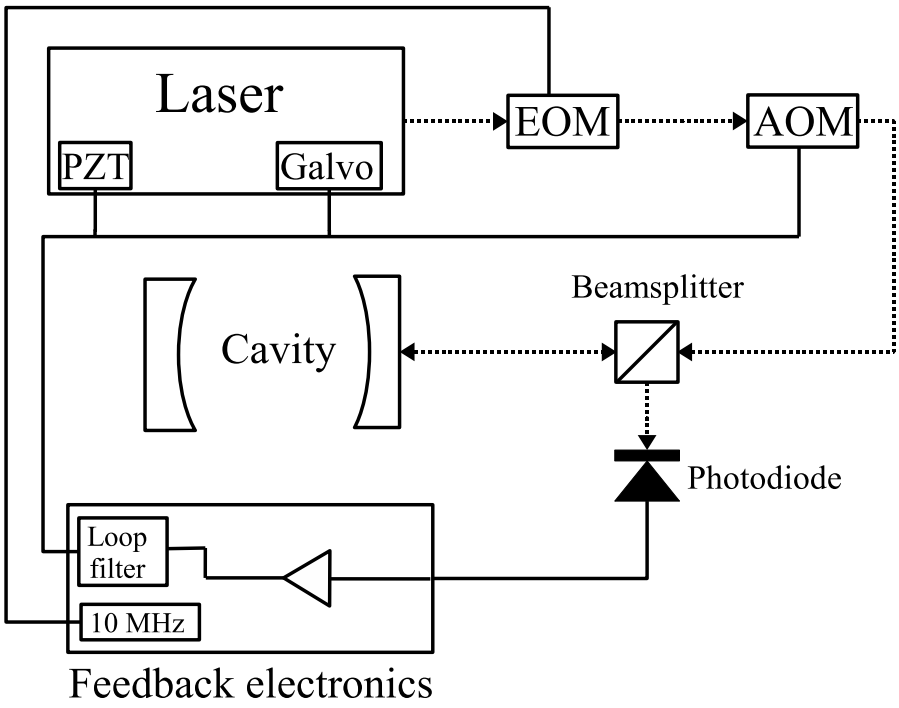

Figure 2: Schematic picture of the main features of the stabilisation setup. Optical connections are represented with dashed lines and electrical connections with solid lines. The 10 MHz signal is used in the phase modulation step at the EOM and is de-modulated in the feedback electronics. The signal to the three frequency correcting servos is actively filtered for their corresponding bandwidths.

Once the frequency stabilisation is activated, the center of the laser frequency is fixed to correspond to one of the transmission maxima of the cavity. This means that a constant DC level is observed at the photodiode that is placed after

the cavity. The ringdown decays are initiated by turning the AOM on and off. A long-travel piezo ceramic tube (up to 30 μm of displacement) is attached to one of the ringdown cavity mirrors in order to enable scanning of the laser frequency. While the feedback loop is closed, the laser follows any frequency changes in the transmission maxima and scanning the cavity length amounts to effectively scanning the frequencies of the cavity fringes. With this configuration, the laser frequency can be scanned by almost one inverse centimeter (about 30 GHz). Repetition rates of up to 20 kHz are possible, although the stability of the lock is somewhat compromised towards the upper end of the scale; a more practical repetition rate is about 10 kHz. The data acquisition problem, mentioned above, is solved with the use of a high-resolution (14 bit) digital-to-analog converter which possesses 8 million samples of on-board memory. The memory is filled once for each point in the spectrum and then transferred to the computer when the laser frequency is changed.

The setup described in Publications IV and V achieves a short term minimum detectable absorption loss (MDAL) of about 1×10^{-11} cm^{-1}Hz$^{-1/2}$. This corresponds to a measurement where 10 000 exponentials are recorded within one second and the standard deviation of the distribution of ringdown times is calculated. The long term sensitivity is, however, worse. This is due to a slow drift of the time constant in the time domain and also to various wavenumber-domain features that change the baseline of the spectra during the ~ 0.9 cm^{-1} scan range. The long term MDAL for the setup is about 9×10^{-11} cm^{-1}Hz$^{-1/2}$.

Our laser-locked setup produces a good short term standard deviation for the time constant. The relative standard deviation is about 0.02% on a day-to-day basis. Other setups around the world seem to produce standard deviations ranging between 1% for typical pulsed-CRDS experiments and down to 0.03% [2, 26] in experiments where single-mode excitation is achieved. A striking exception is the setup of Spence *et al.* [22] that achieves a relative standard deviation of 0.0024% as discussed in Publication IV. This parameter, however, is not always explicitly given in publications and the recording time for the set of data used to evaluate the distribution varies in different setups.

Besides the more efficient averaging and the better timing that our laser-locked approach allows for, the high repetition rate is also convenient for diagnostics of the experimental setup itself. With a rate of 10 000 decays per second the

evolution of the time constant and its distribution can be monitored in real time while aligning the beam path or adjusting the gains of the feedback electronics, for example. It is especially important to monitor the spread of the distribution to make sure that the standard deviation is minimised and that the shape is close to a Gaussian function.

3.1.2 Intra-cavity laser absorption spectroscopy

Intra-cavity laser absorption spectroscopy (ICLAS) is an established technique first pioneered in Russia in the 1970's [27]. Both the experimental and theoretical aspects of ICLAS have been developed extensively since then, and it stands now as one of the most sensitive spectroscopic techniques available for absorption experiments.

In a standard ICLAS experiment, the molecular sample is placed inside a laser cavity that is operated in a broadband configuration with a homogeneously broadened gain medium. Provided that the absorption features of the sample are narrower than the laser spectrum, the dispersed output of the laser beam consists of the envelope of the laser gain profile overlaid with the sample absorption spectrum. While the broadband losses of the cavity are compensated for by the laser gain medium, the narrow absorption peaks of the molecular sample remain in the spectrum and the laser acts effectively as a multi-pass cell without reflection losses [28, 29]. Depending on the time the photons are allowed to interact with the cavity, the effective absorption path length can be extended to up to tens or even thousands of kilometers [30].

The effective path length in an ICLAS experiment can be given as

$$L_{eff} = ct_g \frac{l}{L}, \tag{23}$$

where t_g is the generation time, l is the length of the sample cell and L is the total length of the laser cavity. The quantity t_g is defined as the time elapsed between the start of the laser oscillation and the recording of the output spectrum. This value for the effective path length can be inserted into the standard Lambert-Beer absorption law and, along with the signal-to-noise ratio of the experiment, determines the achievable sensitivity of the setup.

For a proper understanding of the physics involved in the ICLAS experiment, one must study the equation that describes the time evolution of the laser spectrum after the start of the oscillation. The photon numbers M_q in each longitudinal laser mode q are given by [28]

$$M_q(t_g) = M\frac{\sqrt{\gamma t_g/\pi}}{Q}\exp\left[-\left(\frac{q-q_0}{Q}\right)^2\gamma t_g\right]\exp\left(-\alpha_q\frac{l}{L}ct_g\right), \qquad (24)$$

where M is the total photon number, γ is the broadband cavity loss rate, q_0 is the central mode of the gain spectrum, Q is the half-width at the half-maximum of the spectral profile and α_q is the absorption coefficient of the sample at the frequency of mode q.

It is obvious from Eq. 24 that along with the effective increase of path length (the second exponential term) longer generation times also bring a narrowing of the Gaussian laser envelope (as $\sim 1/\sqrt{t_g}$). This means that a single high-sensitivity measurement covers a smaller wavenumber range than a measurement with shorter t_g. The equation is only valid for a limited time interval after the initial turn-on of the laser. At some point, inherent spontaneous emission stops the growth of the absorption lines and the narrowing of the laser spectrum. This stationary spectrum is reached after a time that is characteristic to the laser system and depends on the upper laser level lifetime, beam diameter and homogeneous width of the gain profile [28].

The most straightforward way of conducting an ICLAS experiment is to direct the laser output to a dispersive element, such as a grating spectrograph. When coupled with a CCD-camera, this setup allows for real-time acquisition of laser spectra. The problems with such a system are the poor linearity of the spectrograph and the usually modest spectral resolution achieved with such devices.

One possibility is to replace the dispersing element with a Fourier transform (FT) interferometer [31, 32, 33, 34]. This approach is adopted in Publication III of this thesis. Interferometers possess a better scanning linearity and calibration is therefore easier with fewer points required per spectral region to attach a reliable wavenumber scale to the spectrum. The achievable resolution is also better than that obtained with a spectrograph. Commercial instruments with 0.002 cm^{-1} resolution are available.

An FT-instrument brings some benefits to an ICLAS experiment but there are also problems. One disadvantage is the indirect way in which the interferometer samples the laser spectrum. Each position of the moving mirror corresponds to a different set of analysed frequencies and in principle one is assuming a steady state (time-independent) composition for the spectrum of the source. In the case of FT-ICLAS, the source is a laser and the spectral composition at the time instant t_g is the result of a statistical process. The photon numbers in each of the contributing laser modes are based on a build-up of stimulated emission upon the initial spontaneous emission statistics and the final photon numbers at time t_g are different for each laser shot. Thus, each position of the moving mirror effectively samples a different laser spectrum. This is exacerbated with continuous scan interferometers, where the moving mirror does not advance in discrete steps as it does in a step scan interferometer. In step scan mode, one can average several points for each position of the mirror and the noise contribution of the spontaneous emission is diminished. But even in continuous scan mode, which was used in this work, one is effectively averaging the photon numbers in adjacent laser modes provided that the instrumental resolution is lower than the mode spacing of the laser. The free spectral range of our Ti:Sapphire laser with its 2 meter ring cavity is 150 MHz (0.005 cm^{-1}). This means that with the instrumental resolution of 0.05 cm^{-1}, as used in the experiment described in Article III, about 10 laser modes are averaged for each interferogram point.

Another problem associated with the FT approach is the relatively long time it takes to scan a spectrum in high resolution. In normal FT experiments, this is balanced by the fact that for each scan the whole wavenumber space is sampled whereas in FT-ICLAS one is limited by the narrow wavenumber spread of the laser spectrum. With a spectrograph and a CCD camera, the averaging of the laser shots can be followed in real time and any problems with the laser operation can be observed immediately and be dealt with. Hu *et al.* [33] give equivalent recording times of 1 minute and 1 hour for standard ICLAS and FT-ICLAS experiments, respectively.

To be able to consistently record the laser spectrum at a certain time instant after the beginning of laser action (t_g), some kind of synchronisation scheme must be devised between the FT-instrument and the laser. We inserted an AOM between the pump laser (Coherent Ar-ion laser) and the ring laser to chop the

pump beam. A trigger signal from the electronics of the interferometer controls the phase and frequency of the chop modulation. This control signal corresponds to the actual sampling instant of the analog-to-digital converter used to sample the detector output to form the interferogram. By assuming a constant frequency for the sampling events, one can adjust the phase of the modulation signal to the AOM so that the sampling events occur always with a set delay (t_g) after the pump laser turn-on. This scenario is, however, complicated by the fact that the sampling events of the interferometer are not equally spaced in time but are controlled by the motion of the moving mirror and are only spaced uniformly in the distance space of the mirror. Thus, any instabilities in the mechanical system will end up modulating the sampling frequency. This is not a problem for the operation of the interferometer itself but will result as jitter in the generation times of the laser spectra. The magnitude of this jitter is minor (in the order of a few μs) and will not compromise the overall operation of the FT-ICLAS setup, especially if the absolute value of the generation time is not critical, as is the case in our experiment.

Despite the aforementioned problems, it is demonstrated in Publication III that FT-ICLAS can be realised easily with a commercial laser and an interferometer. The main limiting factor is our Coherent 899-21 Ti:Sapphire ring laser which is designed to be geometrically compact and is not compatible with the long intra-cavity cell that is needed for ICLAS studies. The laser is also optimised for single-mode operation and we encountered problems when recording broadband ICLAS spectra. When the generation time was set to 80 μs or longer, additional noise of unknown origin appeared in the laser spectrum. This limited the achievable sensitivity but the resulting spectra were still of high enough quality to meet our purposes.

3.2 Emission techniques

3.2.1 Dispersed laser-induced infrared fluorescence spectroscopy

A spectroscopist instinctively associates fluorescence with transitions between different electronic states in the same electronic spin manifold. Emittive transitions between vibrational states of the same electronic state are not commonly studied, at least not with coherent sources such as lasers. There is a good reason for this:

The transition moments for vibrational transitions are much smaller than for electronic transitions and therefore, whereas the electronic fluorescence is easily observed, the vibrational emission is not. In addition, detectors are more sensitive in the visible and ultraviolet range, and room temperature blackbody radiation is insignificant unlike in the infrared part of the electromagnetic spectrum.

Even though the vibrational emission transitions are hard to detect, they can reveal molecular information that is not readily available with standard one-photon absorption techniques. This is due to the spectroscopic selection rules associated with symmetric molecules like acetylene where only transitions between symmetric and anti-symmetric vibrational states are allowed. The wavefunction of the ground vibrational state of acetylene is symmetric and other symmetric states can only be observed in direct one-photon absorption experiments as hot bands. Emission transitions involving symmetric states can, however, be recorded directly by first pumping an anti-symmetric state and then observing fluorescence to a symmetric state.

Another avenue for investigation is opened by the fairly long life times exhibited by the rovibrational states. These are in the order of milliseconds, which means that the molecule will experience a number of collisions (in the pressure range used in the experiments) before it loses the excitation energy through spontaneous emission. Thus, even if the frequency of the pump laser is kept fixed and initially only one upper vibration–rotation state is populated, in the end, several states are excited through the collisional energy transfer. This process can lead to population transfer not only to nearby rotational states but also to close lying vibrational states. The collisionally excited vibrational states will be symmetric ones if we assume that the collisional transitions obey the same selection rules as optical transitions. This increases the amount of new molecular information gained from the experiment and at the same time decreases the sensitivity by spreading the excitation energy among several fluorescence transitions.

In the case of the experiment described in Publication II, the spectra of normal acetylene indicated that under the experimental conditions the collisions were efficient enough to effectively quench all the emittive transitions after the first fluorescence ($v = 4 \rightarrow 3$, where v is the C-H stretch quantum number) step. The excitation energy is funneled through collisions to the lowest excited vibrational state available ($v = 1$) before emission to the ground state is observed. Because

most of the molecules inside the sample cell are in the ground vibrational state, there is a possibility for re-absorption with the emitted ($v = 1 \rightarrow 0$) photons absorbed by the $v = 1 \leftarrow 0$ transition. This re-absorption process is indeed observed and also accounts for some peculiarities in the lineshapes of the $v = 1 \rightarrow 0$ transition recorded in Publication II.

The dispersed laser-induced infrared fluorescence (IR-LIF) experiment is instrumentally simple. A cell with a gaseous sample is placed inside the ring laser cavity and the frequency of the laser is tuned to correspond to an absorption feature. The resulting emission is directed to an interferometer, which is used to analyse the spectrum. The intra-cavity configuration is chosen because it optimises the available optical power to efficiently pump the upper states of the fluorescence transitions. A 15 W Argon ion laser is used to optically pump the Ti:Sapphire laser and about 30 W of intra-cavity power is obtained inside the ring laser cavity. This is in contrast to the 2 or 3 W of maximum optical power if the fluorescence experiment were to be conducted outside of the laser cavity. The laser is operated in a single-mode configuration, and this guarantees a linewidth of about 20 MHz. The Doppler-broadened linewidth of acetylene transitions at 12 000 cm^{-1} is about 1 GHz (full-width at half-maximum) at room temperature. This means that only one transition is pumped at a time and any energy transfer to other ro-vibrational states is either collisional or emittive.

An interesting feature of this experimental setup is the collection of the radiation that is sent to the interferometer. The initial experiments in our laboratory used a parabolic mirror in standard manner to collect radiation from its focal point and to collimate it [35, 36, 37, 38]. The laser beam passes through the parabolic mirror (and its focal point) via two holes drilled on the opposite sides of the mirror. It was noticed later on that the emission signal is maximised when, instead of the focal point, the image of the second hole is focused into the interferometer optics. This hole corresponds to the "exit hole" of the travelling wave laser beam. The maximum of the emission signal is obtained with the minimum radius of the hole, as long as the hole is large enough for the laser beam to pass through cleanly. The emitted photons are reflected at the edges of the hole in the mirror and the disadvantage is that they are not collimated like the photons emitted at the focal point. The collection system is depicted schematically in Figure 3. This method of collecting the radiation may seem unusual at first but

is simply a result of the geometry of the laser beam that excites the molecules. The excitation occurs along a line (the beam) and, although the spontaneous emission is omni-directional, the photons that are emitted in the direction of the beam originate from the same axis and are thus easier to collect. All the other directions will have the same amount of photons but the ones that are emitted on the beam path will actually direct to the same point or at least the same small area. The reverse path, on the other hand, should be equivalent with the forward path and the emission intensity should be identical at the edges of the "entry hole". This is, however, difficult to experimentally verify since we have relied on the weak reflections of the laser beam itself to align the infrared emission to the interferometer. There are no such reflections coming from the edges of the "entry hole".

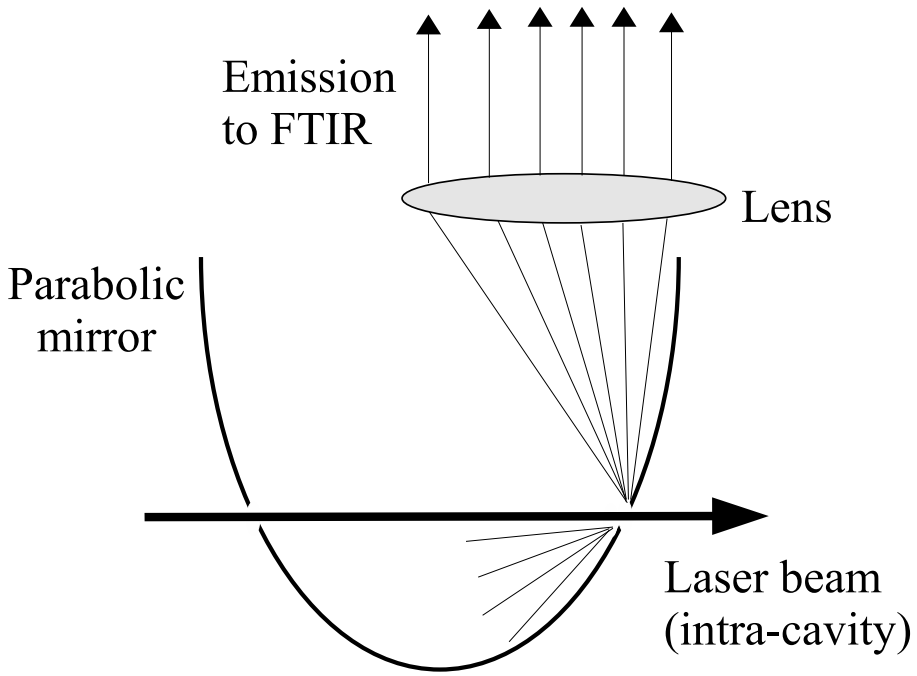

Figure 3: Schematic picture of the optical collection scheme in the dispersed infrared fluorescence setup. A parabolic mirror is inserted inside the ring laser cavity with holes to accommodate the beam passage. Emission is gathered as reflections from around the exit hole of the beam. The radiation is collimated with a lens and sent to the interferometer.

Another interesting feature of the fluorescence spectra is the intensity distribution of the observed peaks. Two of the peaks, corresponding to $\Delta J = \pm 1$

transitions, are much stronger than the rest. That is, the state directly pumped by the laser beam retains most of the excitation energy while the collision-populated states are excited to a lesser extent. This would seem to indicate that the molecular sample does not have time to reach an equilibrium state where the collisions would re-distribute the energy according to the Boltzmann principle. However, a simple kinetic theory calculation for the number of collisions per time unit for a molecule in the experimental conditions points to a different direction. Assuming a molar mass of 26 g/mol (HCCH) and a collisional cross section of 0.5 nm^2 for 1 mbar ambient pressure and room temperature, the collision frequency is about 8×10^6 Hz (or 125 ns between collisions). For an assumed upper state radiative lifetime of about one millisecond, the molecule should have ample time to collide with its neighbours and to distribute the excitation energy to reach an equilibrium state. The spectra in Article II are in disagreement with this argument and the reason for this discrepancy can be explained by the experimental configuration we have used for the collection of fluorescence.

As mentioned above, the emission is collected from the edges of a hole that is drilled through the parabolic mirror to allow the laser beam to exit. The photons that are directed to the interferometer are actually those that have been emitted in the direction of the beam as it passes through the sample cell. It now seems reasonable that only those excited molecules that have not had time to move out of the beam (or close vicinity of it) would contribute to the collected emission. That is, only a small portion of the total number of excited molecules emit along a suitable direction for the collection optics to recover the photons. The mean speed of acetylene molecules at room temperature is about 500 m/s and the diameter of the laser beam is less than 1 mm. This means that an average molecule will pass through the beam (if it crosses the beam at a right angle) in about 2 μs. This is three orders of magnitude less than the assumed lifetime of the upper state and only one order of magnitude more than the time between molecular collisions. Thus, it seems that the molecules from which emission is recorded do not have time to collide extensively with their neighbours. This explains the observed intensity distribution qualitatively and confirms that our experiment samples most effectively only those excited molecules that happen to emit shortly after the excitation. Of course, some of the molecules that leave the beam will return back to the volume occupied by the beam before they have

emitted the radiation but as the volume of the sample cell is large compared to the beam this effect is probably only a minor one.

All the spectra of normal acetylene recorded by the IR-LIF setup conserve the nuclear spin state. That is, if an *ortho* (the total nuclear spin quantum number $I = 1$) state is pumped, the emission lines belong exclusively to the *ortho* manifold, and the same applies for the *para* ($I = 0$) states. However, for rovibrational states that contain substantial *ortho-para* mixing, there is a possibility of enhanced nuclear spin conversion initiated by collision processes [39]. Interestingly, there are reports in the literature about experimental observations of *ortho* to *para* spin conversion within the 1030^00^0 vibrational state of acetylene [40], a state which is pumped in the IR-LIF experiment described in Publication II. The experimental technique used in the study in question (time-resolved infrared-ultraviolet double resonance spectroscopy) is, however, more complicated than the IR-LIF experiment and it is possible that the apparent observation of *ortho* to *para* conversion is related to experimental complexities that mask the real processes occurring in the sample. In fact, later studies published by the same group attributed the observed anomalous transitions to phenomena other than nuclear spin conversion [41].

4 Conclusions

The main results in this study are the different experimental setups that have been realised in the laboratory. These include the standard cw-CRDS experiment, the enhanced version of the dispersed infrared fluorescence setup, the FT-ICLAS apparatus and finally the laser-locked cw-CRDS experiment with high speed data acquisition system. Of these, the dispersed fluorescence setup is unique in the world and the laser-locked CRDS experiment has not been realised anywhere else with such broad spectral tunability, making the instrument a real spectroscopic tool for high-sensitivity measurements.

Besides the developments in the instrumental sector, I have applied the techniques to molecular systems, measuring the overtone spectra of acetylene and its isotopologues. Thus, this study has also produced molecular data on the rotational and vibrational energy level structure of these molecules. These results are summarised in Table 2, where all the vibrational bands observed in this study are

collected. Especially noteworthy are the data on symmetric vibrational states of normal acetylene that have been recorded with the dispersed infrared fluorescence setup. These kind of states are not accessible as one-photon absorption transitions from the ground vibrational state and the amount of information available on them is scarce.

One clear avenue for further research is the application of the laser stabilisation system to the laser-induced infrared fluorescence experiment. The Fabry-Perót cavity that is used as a frequency reference builds up a large amount of optical power between its mirrors and this power could be used to pump the upper states more efficiently that can be done with the intra-cavity setup. The power build-up factor is ideally $1/(1-R)$ [43] which would mean a circulating power of about 5000 times the input power for the cavity used in this thesis. The fluorescence emission could be collected along the beam path, outside the cavity, after suitable filtering of the laser beam itself. One problem with this setup might be the delicate nature of the dielectric mirror coatings. If high intra-cavity powers are used, the performance of the mirrors may degrade due to thermal effects within the coatings. If accomplished, the high pumping power offered by the build-up cavity would increase the signal-to-noise ratio of the dispersed infrared fluorescence experiment significantly. This would make the technique more widely applicable and one could probe weaker overtone transitions than the acetylene bands studied in Publication II. Another possible candidate would be methane, which is highly symmetric and therefore possesses states that cannot be accessed directly from the ground vibrational state. In fact, we tried the intra-cavity fluorescence experiment with the strongest overtone transition in the range of the Ti:Sapphire laser and observed no fluorescence. This experiment might be feasible with a better sensitivity enabled by the build-up cavity.

The laser-locked CRDS setup is a versatile tool for further ultra-sensitive absorption measurements. In addition to this, it might be a useful instrument when used as a detector in reaction kinetics experiments. CRDS has previously been utilised in kinetic studies and the high repetition rate achieved for the ringdown events in our laser-locked setup may prove useful in this context. Faster reactions with shorter lifetimes could be followed and the high sensitivity of the setup would also be useful. The synchronisation between the start of the reaction and the measurement of ringdown events is also easier to accomplish in

a locked cw-CRDS experiment than it is in the standard cw-CRDS setup. Sub-Doppler experiments might also be possible with the stabilised laser setup. The large optical power inside the external cavity could be used to saturate molecular transitions and the standing-wave configuration lends itself to observing Lamb dips in the inhomogeneously broadened Doppler-profiles of room temperature gas samples [44].

Molecule	State		G /cm^{-1}	B /cm^{-1}	$10^6 D$ /cm^{-1}	$10^8 H$ /cm^{-1}
$H^{12}C^{12}CH$	0120^00^0	Σ_g^+	8467.3374(44)	1.15909(11)	1.35(58)	
	1204^00^0	Σ_g^+	9618.5984(76)	1.16240(17)	-6.86(89)	
	1204^00^0	Σ_g^+	9637.7150(50)	1.16235(15)	-16.89(92)	
	1020^00^0	Σ_g^+	9663.3860(11)	1.158053(16)	1.742(38)	
	1120^00^0	Σ_g^+	11611.8905(50)	1.15168(10)	1.15(41)	
	1120^01^1	$\Pi_u(e)$	12311.8152(17)	1.151899(32)	0.37(12)	
	1120^01^1	$\Pi_u(f)$	12311.8228(15)	1.156326(19)	1.246(43)	
	2111^10^0	$\Pi_u(e)$	12350.5953(10)	1.150550(18)	1.649(59)	
	2111^10^0	$\Pi_u(f)$	12350.6023(17)	1.156085(27)	1.616(74)	
	0040^00^0	Σ_g^+	12671.6252(13)	1.151529(17)	1.712(40)	
$H^{12}C^{13}CH$		Σ^+	12608.9968(28)	1.13157(18)	−20.8(11)	−3.63(18)
		Σ^+	12613.79(39)	1.1651(54)	139(22)	19.0(32)
	0040^00^0	Σ^+	12617.495(12)	1.12590(30)	−11.4(47)	−1.31(82)
		Σ^+	12665.0806(45)	1.128955(82)	−9.81(37)	−1.138(46)
	1030^00^0	Σ^+	12672.2678(28)	1.125720(43)	2.88(15)	0.642(15)
		Σ^+	12682.3618(54)	1.12910(10)	−1.24(33)	
$H^{13}C^{13}CH$		$\Pi_u(e)$	11961.1405(32)[a]	1.09457(13)	−13.4(10)	
		$\Pi_u(f)$	11961.1652(55)[a]	1.10253(20)	−7.6(14)	
	1310^00^0	Σ_u^+	12169.35138(51)	1.0908535(31)	1.4668(33)	
	1302^03^1	$\Pi_u(e)$	12190.16176(98)	1.097310(12)	2.410(26)	
	1302^03^1	$\Pi_u(f)$	12190.17151(75)	1.1092024(52)	3.8122(65)	
	1120^01^1	$\Pi_u(e)$	12204.8745(11)	1.0965372(87)	1.800(12)	
	1120^01^1	$\Pi_u(f)$	12204.8794(11)	1.102788(16)	1.212(44)	
	2202^21^{-1}	$\Pi_u(e)$	12228.41588(71)	1.0969912(72)	1.140(14)	
	2202^21^{-1}	$\Pi_u(f)$	12228.4209(13)	1.1028645(90)	1.887(12)	
		Σ_u^+	12605.542(58)	1.11496(27)		
		Σ_u^+	12606.387(74)	1.10307(17)		
	1030^00^0	Σ_u^+	12609.2489(44)	1.098055(72)	4.31(26)	
	0132^00^0	Σ_u^+	12628.8213(16)	1.097833(22)	0.234(71)	6.85(60)

See Table 1 for the normal mode notation used for the vibrational assignments. The quantity G is the vibrational term value. Vibrational assignments for the states are given when available. Assignments are presented as the eigenstate with the highest percentage of contribution. See the corresponding publication for details. Numbers in parentheses following a numerical value for a molecular parameter represent one-standard deviation in the least significant digit.
[a] Observed as a hot band. Lower state energy (602.7674 cm^{-1}) [42] deducted from the experimentally observed vibrational term value.

Table 2: Vibrational states of acetylene observed and rotationally analysed in this study

Errata

Publication I

1. *The value for free spectral range of the cavity on page 375 should read* 466 MHz.

2. *The vibrational assignment for state at 12 311.8 cm^{-1} given in Table I, page 376, should read* $1120^0 1^1$.

Publication V

1. *The correct citation for Ref. 6 is* R. W. P. Drever, J. L. Hall, F. W. Kowalski, J. Hough, G. M. Ford, A. J. Munley and H. Ward, Appl. Phys. B **31** (1983) 97. *(Corrected in proof)*

References

[1] M. W. Todd, R. A. Provencal, T. G. Owano, B. A. Paldus, A. Kachanov, K. L. Vodopyanov, M. Hunter, S. L. Coy, J. I. Steinfeld and J. T. Arnold, Appl. Phys. B **75**, 367 (2002).

[2] E. R. Crosson, K. N. Ricci, B. A. Richman, F. C. Chilese, T. G. Owano, R. A. Provencal, M. W. Todd, J. Glasser, A. A. Kachanov, B. A. Paldus, T. G. Spence and R. N. Zare, Anal. Chem **74**, 2003 (2002).

[3] H. Dahnke, D. Kleine, P. Hering and M. Mürtz, Appl. Phys. B **72**, 971 (2001).

[4] E. Wahl, S. Tan, S. Koulikov, B. Kharlamov, C. Rella, E. Crosson, D. Biswell and B. Paldus, Opt. Express **14**, 1673 (2006).

[5] P. B. Tarsa, P. Rabinowitz and K. K. Lehmann, Chemical Physics Letters **383**, 297 (2004).

[6] K. L. Snyder and R. N. Zare, Anal. Chem. **75**, 3086 (2003).

[7] M. Herman, J. Lievin, J. Vander Auwera and A. Campargue, Adv. Chem. Phys. **108**, 1 (1999).

[8] G. Di Lonardo, L. Fusina, E. Venuti, J. W. C. Johns, M. I. El Idrissi, J. Lievin and M. Herman, J. Chem. Phys. **111**, 1008 (1999).

[9] P. W. Atkins and R. S. Friedman, *Molecular Quantum Mechanics* (Oxford University Press, Oxford, 1997).

[10] G. Herzberg, *Molecular Spectra and Molecular Structure II. Infrared and Raman Spectra of Polyatomic Molecules* (Van Nostrand, New York, 1945).

[11] J. M. Hollas, *Modern Spectroscopy* (John Wiley & Sons, Chichester, 1996).

[12] M. S. Child and L. Halonen, Adv. Chem. Phys. **57**, 1 (1984).

[13] M. J. Bramley and N. C. Handy, J. Chem. Phys. **98**, 1378 (1993).

[14] P.F. Bernath, *Spectra of Atoms and Molecules* (Oxford University Press, New York, 2005).

[15] P. R. Griffiths and J. A. de Haseth, *Fourier Transform Infrared Spectrometry*, Chemical Analysis, vol. 83 (John Wiley & Sons, Chichester, 1986).

[16] A. O'Keefe and D. A. G. Deacon, Rev. Sci. Instrum. **59**, 2544 (1988).

[17] G. Berden, R. Peeters and G. Meijer, Int. Rev. Phys. Chem. **19**, 565 (2000).

[18] E. Hecht, *Optics* (Addison-Wesley, New York, 1998).

[19] K. K. Lehmann and D. Romanini, J. Chem. Phys. **105**, 10263 (1996).

[20] D. Romanini, A. A. Kachanov, N. Sadeghi and F. Stoeckel, Chem. Phys. Lett. **264**, 316 (1997).

[21] D. Romanini and K. K. Lehmann, J. Chem. Phys. **99**, 6287 (1993).

[22] T. G. Spence, C. C. Harb, B. A. Paldus, R. N. Zare, B. Wilkie and R. L. Byer, Rev. Sci. Instrum. **71**, 347 (2000).

[23] N. J. van Leeuwen, J. C. Diettrich and A. C. Wilson, Appl. Opt. **42**, 3670 (2003).

[24] R. L. Barger, M. S. Sorem and J. L. Hall, Appl. Phys. **22**, 573 (1973).

[25] R. W. P. Drever, J. L. Hall, F. W. Kowalski, J. Hough, G. M. Ford, A. J. Munley and H. Ward, Appl. Phys. B **31**, 97 (1983).

[26] R. D. van Zee, J. T. Hodges and J. P. Looney, Appl. Opt **38**, 3951 (1999).

[27] L. A. Pakhomycheva, E. A. Sviridenkov, A. F. Suchkov, L. V. Titova and S. S. Churilov, JETP Lett. **12**, 43 (1970).

[28] A. Kachanov, A. Charvat and F. Stoeckel, J. Opt. Soc. Am. B **11**, 2412 (1994).

[29] A. Kachanov, A. Charvat and F. Stoeckel, J. Opt. Soc. Am. B **12**, 970 (1995).

[30] S. E. Vinogradov, A. A. Kachanov, S. A. Kovalenko and E. A. Sviridenkov, JETP Lett. **55**, 581 (1992).

[31] C. Domingo, A. del Olmo, R. Escribano, D. Bermejo and J. M. Orza, J. Chem. Phys. **96**, 972 (1992).

[32] S. Hu, H. Lin, S. He, J. Cheng and Q. Zhu, Phys. Chem. Chem. Phys. **1**, 3727 (1999).

[33] S.-M. Hu, A. Campargue, Z.-Y. Wu, Y. Ding, A.-W. Liu and Q. Zhu, Chem. Phys. Lett. **372**, 659 (2003).

[34] S. Kassi, C. Depiesse, M. Herman and D. Hurtmans, Mol. Phys. **101**, 1155 (2003).

[35] P. Jungner and L. Halonen, J. Chem. Phys. **107**, 1680 (1997).

[36] M. Saarinen, D. Permogorov and L. Halonen, J. Chem. Phys. **110**, 1424 (1999).

[37] M. Nela, D. Permogorov, A. Miani and L. Halonen, J. Chem. Phys. **113**, 1795 (2000).

[38] M. Metsälä, M. Nela, S. Yang, O. Vaittinen and L. Halonen, Vib. Spectrosc. **29**, 155 (2002).

[39] R. F. Curl, Jr., V. V. Kasper and K. S. Pitzer, J. Chem. Phys. **46**, 3220 (1967).

[40] M. A. Payne, A. P. Milce, M. J. Frost and B. J. Orr, Chem. Phys. Lett. **265**, 244 (1997).

[41] M. A. Payne, A. P. Milce, M. J. Frost and B. J. Orr, Chem. Phys. Lett. **324**, 48 (2000).

[42] G. Di Lonardo, P. Ferracuti, L. Fusina, E. Venuti and J. W. C. Johns, J. Mol. Spectrosc. **161**, 466 (1993).

[43] A. E. Siegman, *Lasers* (University Science Books, Mill Valley, CA, 1986).

[44] W. Demtröder, *Laser Spectroscopy* (Springer-Verlag, Berlin, 1998).